



# Pre-stressing aluminum nanoparticles as a strategy to enhance reactivity of nanothermite composites

Rohit J. Jacob<sup>a,c,\*</sup>, Kevin J. Hill<sup>b</sup>, Yong Yang<sup>a</sup>, Michelle L. Pantoya<sup>b</sup>, Michael R. Zachariah<sup>a,\*\*</sup>

<sup>a</sup> Department of Chemical and Biomolecular Engineering, University of Maryland, College Park, MD 20742, USA

<sup>b</sup> Department of Mechanical Engineering, Texas Tech University, Lubbock, TX 79409, USA

<sup>c</sup> National Research Council, The National Academies of Sciences, Engineering and Medicine, 500 fifth Street NW, Washington, DC 20001, USA

## ARTICLE INFO

### Article history:

Received 9 November 2018

Revised 1 December 2018

Accepted 19 March 2019

### Keywords:

Nanoaluminum  
Prestressing  
Combustion  
Reactive sintering  
XRD

## ABSTRACT

Aluminum (Al) fuel particles are used in a variety of energetic formulations yet harvesting their full chemical potential energy and increasing their energy release rate upon ignition have been a challenge and are key motivators to advancing energy generation technologies. One approach to improving combustion performance is to alter the mechanical properties of the Al particle by inducing an elevated stress state through prestressing. This study examines the combustion performance of prestressed nanoscale aluminum (nAl) particles that were annealed to temperatures ranging from 200 to 400 °C and quenched at slow (exponential) and faster (linear) cooling rates. Powder X-ray diffraction measurements show that prestressing nAl particles at 300 °C increases the strain by an order of magnitude. Constant volume combustion cell tests on nAl combined with copper oxide nanopowder (nAl + CuO) revealed higher peak pressures and pressurization rates for prestressed nAl + CuO composites compared to their untreated counterpart. High speed emission spectroscopy was employed to deduce condensed phase temperatures from the reaction confined within the combustion cell. Burn time measurements, obtained by integrating the emission spectra, were observed to correlate inversely with generated pressure. High heating rate ( $\sim 5 \times 10^5$  K/s) *in-situ* TEM results augment the combustion cell results. The results imply that prestressing mechanically alters the nanoparticles which subsequently accelerate the release of aluminum core through outward diffusion. This results in the rapid loss of nanostructure which was observed at the nanoscale through *in-situ* electron microscopy. The released aluminum thus reacts rapidly with the oxidizer in the condensed phase resulting in a faster and more violent reaction. Improved performance of prestressed nAl coupled with the simplicity of processing provides a low cost and scalable approach to improving metal fuel particle combustion.

© 2019 The Combustion Institute. Published by Elsevier Inc. All rights reserved.

## 1. Introduction

Nanotechnology has facilitated significant developments in the field of metalized energetic materials, which have been historically plagued by poor reactivity and incomplete combustion [1]. With the objective of approaching the fast reactivity of traditional monomolecular explosives, while maintaining the microstructural and compositional tunability of a composite, a new class of nanoparticulate energetic materials termed ‘Metastable Intermolecular Composites’ (MIC’s) was developed to harvest the exothermic redox reaction in a condensed phase metal-oxidizer system. MIC

research gained significant traction in recent years owing to their high energy density, tunability, and reactivity [2], with reports highlighting a three order of magnitude improvement in burn rate over conventional micron scale materials.

Aluminum is a fuel of choice owing to its availability, low cost, high energy density and environmentally benign reaction products although other metallic fuels such as boron, titanium and tantalum [2] are also being investigated. Conventional wisdom advocates that the reactivity scales inversely with particle size, owing to a reduction in the diffusion length scales for the reactants. Although this hypothesis has proven true for metal particle combustion in the micron scale [3] to early nanoscale (100s of nm) [4], further reduction of the primary particle size in the nano-regime has produced diminished returns in terms of reactivity [5]. Nanoaluminum (nAl) naturally develops a 3–5 nm alumina shell [6] upon exposure to oxygen, whose contribution to the total particle mass increases as the particle size is reduced leading to reduced active aluminum

\* Corresponding author at: Department of Chemical and Biomolecular Engineering, University of Maryland, College Park, MD 20742, USA.

\*\* Corresponding author.

E-mail addresses: [rohit.jacob.ctr@nrl.navy.mil](mailto:rohit.jacob.ctr@nrl.navy.mil) (R.J. Jacob), [mrz@umd.edu](mailto:mrz@umd.edu) (M.R. Zachariah).

content at smaller particle sizes, contributing to the aforementioned reduction in reactivity [7]. Another reason for the reduction in reactive potential is the role of inter-particle sintering whereby at high temperatures, highly aggregated nanoparticles coalesce rapidly on a time scale faster than energy release and effectively reduce the advantage of employing nanoscale materials [8–10].

The role of the inert alumina layer on the overall reaction dynamics of nAl has been a subject of intense debate over the years because the layer presents a barrier to the interaction of aluminum with the oxidizer [11]. Several theories have been proposed to identify the dynamics of the core-shell interface and its significance to the reactivity of the nano composite, with the mechanochemical Melt Dispersion Mechanism (MDM) [12] and the condensed phase diffusion mechanism being the most prominent. MDM predicated on the catastrophic spallation of the molten core upon failure of the shell at very high heating rates ( $\sim 10^6$ – $10^8$  K/s), resulting in the released aluminum clusters undergoing a kinetically limited reaction with the oxidizer. The diffusion mechanism, contrarily, proposes the condensed phase transfer of Al ions across the phase transformed alumina shell as the reason for fast reactivity [11,13]. Recent high spatio-temporal resolution experiments on nanoscale aluminum with copper oxide (nAl + CuO) reaction in a dynamic Transmission Electron Microscope (TEM) revealed the predominance of a condensed phase diffusion mechanism where the reactant moieties were observed to rapidly coalesce ( $< 1 \mu\text{s}$ ) to larger characteristic dimensions resulting in an increase in diffusion length scales and thereby not achieving complete combustion [14–16].

Attempts at improving the reactivity of nanoscale energetic materials (NEMs) can be broadly classified into either altering the mesoscale architecture/assembly of fuel and oxidizer moieties (improved mixing) [17,18] or altering the performance/properties of the fuel to facilitate more rapid introduction of fuel. The latter method, the focus of this work, has been aided by the recent development in synthesis routes leading to the production of intermetallic fuels [19], multi-metal fuels [20,21], oxide free nAl passivated with carboxylic acids [22] and surface functionalized nanoparticles with oxidizers [23]. With the objective of accelerating the participation of aluminum in reaction, this work focuses on another strategy where commercial nAl powder is annealed and quenched to alter the dilatational strain and stress at the core-shell particle interface in order to expedite the release of aluminum during reaction. Prestressing involves annealing the nAl powder at a fixed temperature followed by quenching at a preset cooling rate. This strategy affords the use of commercially available nanoparticles and has the advantage of bulk processing as opposed to the wet chemistry techniques that usually have poor yield [24] and significant impurities [25].

Recent experiments demonstrated the advantages of prestressing micron scale aluminum powders (5  $\mu\text{m}$  diameter) where flame speeds improved by  $\sim 25\%$  for samples annealed at 300  $^\circ\text{C}$  [26]. No significant dependence on cooling rate was observed in that study, although cooling rates studied were rather slow for traditional metallurgical processing. Through X-Ray diffraction measurements, the heightened flame speed was correlated to an order of magnitude increase in the dilatational strain of the aluminum core which may have led to larger grain sizes and reduced hardness [26,27]. Other studies used nAl powder and revealed 30% improvement in flame speed when nAl combined with molybdenum trioxide (nAl+MoO<sub>3</sub>) composites were annealed at only 105  $^\circ\text{C}$  in argon. The improvement was theoretically explained to be the result of the prestressing procedure introducing compressive stress in the alumina shell and tensile stress in the aluminum core (i.e., opposite to what is manifested upon heating) thereby delaying shell fracture and resulting in faster release of molten aluminum clusters [28]. For these nAl composites, the adopted quench regime

demonstrated a noticeable effect on flame speed with a 14% improvement reported when the cooling rate was increased from 0.06  $^\circ\text{C/s}$  to 0.13  $^\circ\text{C/s}$ . At even higher cooling rates (0.33  $^\circ\text{C/s}$ ), the nAl powder that was annealed with MoO<sub>3</sub> was observed to spontaneously ignite, highlighting the drastic improvement in reactivity [29].

High resolution hot stage TEM experiments conducted on nanoscale aluminum particles revealed that the aluminum core at room temperature exists in a pre-expanded state and that it passes through a zero-strain state at  $\sim 300$   $^\circ\text{C}$ , with further increase in temperature leading to an almost unconstrained expansion of the core [30]. The 300  $^\circ\text{C}$  zero-strain state measurement in nAl particles coincides well with theory for stress relief of residual stress. Timoshenko and others [31–33] suggest that significant microstructural changes take place that promote stress relief at about two-thirds the temperature at which the stresses were formed. In the case of nAl particles, the amorphous alumina shell begins to form at temperatures as high as 440  $^\circ\text{C}$  (i.e., when oxygen is introduced into the inert gas stream as molten Al droplets solidify and at temperatures favoring amorphous alumina formation) [34,35]. Therefore, annealing temperatures should at least be 293  $^\circ\text{C}$  to eliminate residual stress within particles prior to the introduction of more favorable stress (that can be induced with quenching). Beyond 300  $^\circ\text{C}$  the unconstrained expansion of the core was attributed to the inhomogeneous crystallization of the amorphous alumina, which prevented pressure build up from an expanding core [30] thereby aiding the aluminum to leak through imperfections in the inhomogeneous shell. The results were corroborated with high resolution images depicting the release of aluminum and loss of nanostructure with increasing temperature.

Based on existing results, there is merit in annealing aluminum particles prior to combustion for enhanced performance. In this study we embark on a systematic analysis of the combustion performance of nAl annealed to various temperatures and quenched at two different rates. The model composition employed is nAl combined with copper oxide nanopowder (nAl+CuO), which is a highly investigated nanothermite. In fact, nAl+CuO has been shown to produce significant quantities of gaseous oxygen due to the decomposition of CuO, leading to a proposed two-stage reaction mechanism where condensed phase ion transport is responsible for ignition followed by gas phase reaction of aluminum with oxygen [36]. In this study, we employ high speed emission spectroscopy and pressure measurements to quantify the combustion performance of prestressed nAl composites and use high heating rate *in-situ* TEM to mechanistically augment the combustion results. Additionally, the strain associated with selected prestressed nAl particles is measured with powder X-ray diffraction in order to aid the mechanistic discussion associated with reactive performance.

## 2. Experimental

### 2.1. Materials and preparation

Commercial aluminum nanopowder (Novacentrix, Austin, TX) with a primary particle diameter of  $\sim 80$  nm and active aluminum content of  $\sim 80$  wt.% was used in this study. The nanoparticles are manufactured using inert gas condensation following plasma heating of the target material [37]. During synthesis, the generated nanoparticles are exposed to a controlled oxygenated environment which results in the development of a  $\sim 4$  nm thin amorphous oxide shell, as shown in the supplemental section (Fig. S1). The as-purchased aluminum was prestressed by subjecting it to a highly controlled thermal environment using a Q800 Dynamic Mechanical Analyzer (DMA, TA instruments). Three sample batches at annealing temperatures of 200, 300 and 400  $^\circ\text{C}$  were prepared with the samples heated at 10  $^\circ\text{C/min}$  to the annealing temperature and

held at the annealing temperature for 15 min in an inert nitrogen environment. Once annealed, two different cooling routines were employed to gauge the effect of cooling rate on reactivity, as outlined in [6] but summarized below. It is noted that the annealing and quenching process does not appear to alter the size distribution of the powders [38].

The first cooling condition (called exponential cooling) approximated lumped capacitance cooling governed by Eq. (1).

$$T = T_a + (T_0 - T_a) \exp(-At) \quad (1)$$

In Eq. (1)  $T$  is the temperature of the sample,  $T_a$  is the ambient temperature (25 °C),  $T_0$  is the annealing temperature,  $t$  is time, and  $A$  governs the exponential decay from the lumped capacitance model. In all cases,  $A$  is constant at  $0.0078 \text{ s}^{-1}$ .

The second cooling condition (called linear cooling) was a linear rate from the annealing temperature governed by Eq. (2).

$$T = T_0 - Bt \quad (2)$$

In Eq. (2),  $T$ ,  $T_0$ , and  $t$  are defined the same as for the lumped capacitance case, while  $B$  is the linear cooling rate. For each annealing temperature,  $B$  is held constant at  $3.33 \text{ °C/s}$  ( $200 \text{ °C/min}$ ), which is the maximum cooling rate the DMA could supply.

Detailed description of the preparation of nanothermite composites can be found elsewhere [39]. Briefly, a known amount of copper oxide nanopowder (Sigma Aldrich, <100 nm) was dispersed in a vial containing 10 ml of isopropyl alcohol (IPA, Pharmco-Aaper, 99.9%) and sonicated in an ultrasonic bath for 1 h. To this mixture, a stoichiometric amount of the prestressed or untreated aluminum nanopowder was added to make 200 mg of total mixture mass, and the slurry was further sonicated for 1 h. The IPA acts as a process control agent (PCA) which disperses the nanoparticles in solution to achieve intimate mixing, while also preventing accidental ignition. The sonicated mixtures were dried in a fume hood for 24 h to evaporate the solvent. The resulting dry mixture was broken up using a grounded spatula to achieve fine consistency. The combustion performance of the prestressed nAl combined with CuO was tested and compared to the baseline combustion performance of untreated nAl-CuO.

## 2.2. Constant volume pressure cell and high-speed emission spectrometer

Detailed description of the diagnostics used in this work can be found in a recently published article [39]. Briefly, ~25 mg of the nanothermite composite is loaded into a constant volume combustion cell (~20 cc free volume) and ignited using a nichrome wire. The combustion cell is placed in an inert argon environment to minimize the influence of atmospheric oxygen on combustion. The various ports on the cell are coupled separately to a high frequency pressure transducer (PCB Piezoelectric), a broadband PMT (Hamamatsu R13456), and a high speed 32 channel emission spectrometer, as shown in Fig. S2. The pressure transducer and the broadband PMT are terminated to an oscilloscope (Teledyne LeCroy WaveSurfer 3000) which measures the pressure and optical emission from the reacting composite with a temporal resolution of 200 ns. The spectrometer (Acton SP 500i) collects and disperses the emission spectra over a band of 464–867 nm using a 150 groove/mm grating, which is subsequently imaged onto a 32 channel PMT (Hamamatsu H7260) and sampled at ~385 kHz using a high-speed data acquisition system (Vertilon IQSP 580). The wavelength and intensity calibration was performed as outlined in [39], following which the corrected spectra was fit to Planck's law incorporating a grey body assumption to obtain the condensed phase flame temperatures with an error threshold of  $\pm 350 \text{ °C}$  [40,41]. Channels overlapping with significant molecular emission species (such as Na doublet, AlO bands, etc.) were removed using a

custom-built MATLAB [42] fitting routine. Each sample was tested in quadruplicate to ensure repeatability, out of which any significant outliers ( $>3\times$  standard deviations) were removed from the data analysis.

## 2.3. In-situ high heating rate electron microscopy

Owing to the fast reactivity of these composites, high heating rate diagnostics are paramount to probe the underlying initiation dynamics of these materials subjected to ignition. Accordingly, the prestressed nAl particles that demonstrated the best performance in the combustion cell tests were tested in a transmission electron microscope (TEM, JEM 2100 Lab6) to obtain high resolution images. The samples were tested *in-situ* using a specially designed probe (Protochips Aduro) capable of sustaining a rapid thermal pulse at very high heating rates ( $\sim 5 \times 10^5 \text{ °C/s}$ ), commensurate with the dynamics of an actual reaction front [43]. The nAl slurries (without oxidizer) were drop cast onto custom made TEM grids and subjected to a thermal ramp up to 1200 °C. The modularity of the probe allows a choice of final temperatures as well as hold time, and high-resolution images were captured before and after heating to compare and draw conclusions about the reaction mechanism.

## 2.4. Powder X-ray diffraction

Because the internal stress manifested after annealing and quenching are important to understand the reactivity of prestressed nAl particles, X-ray diffraction was employed to examine the best performing nAl samples. A Bruker D5005 X-ray diffractometer was used (with a 0.5 mm divergence slit, a 0.1 mm receiving slit, Cu K $\alpha$  radiation at 40 kV and 30 mA, and a sample diameter of 2.54 cm), and each sample was scanned at  $0.01^\circ$  steps and at 30 s/step. Only the 111, 200, and 220 peaks were probed and analyzed because they are the most expressed.

## 3. Results

### 3.1. High speed pressure and temperature measurements

The performance of the various composites in the combustion cell is presented in Fig. 1, where the effect of prestressing on combustion performance is shown as a function of annealing temperature and quench regime. The pressurization rate was measured by dividing the first prominent pressure peak (10% prominence) by the time elapsed from ignition. Figure 1a show the peak pressure measured for these samples as a function of the prestressing and it can be seen that all prestressing conditions result in improved peak pressure compared to untreated nAl composites, with the most prominent improvement occurring for samples annealed to 300 °C and linearly cooled (~30% improvement in peak pressure). In general, peak pressures exhibit a dependence on the cooling regime with faster, linear quenching resulting in the composites attaining a higher peak pressure. Although there is significant overlap of the 95% confidence bounds in the data presented in Fig. 1a, the statistical significance of improved performance with prestressing has been examined and is presented in the supplemental section for brevity. The pressurization rate (Fig. 1b) for samples annealed at 200 and 300 °C was nearly identical (average values within 5%) and showed only slight improvement for faster quench rates. For the samples annealed at 400 °C, the pressure metrics were significantly diminished compared to 300 °C case with the peak pressure values being similar ( $\sim 1.1\times$ ) to that of the untreated case. The pressurization rate, although lower than the 300 °C samples, was still  $\sim 6$  times that observed for untreated samples. The lower pressure metrics at 400 °C annealing suggest a shift in the reaction mechanism given that the shell may begin

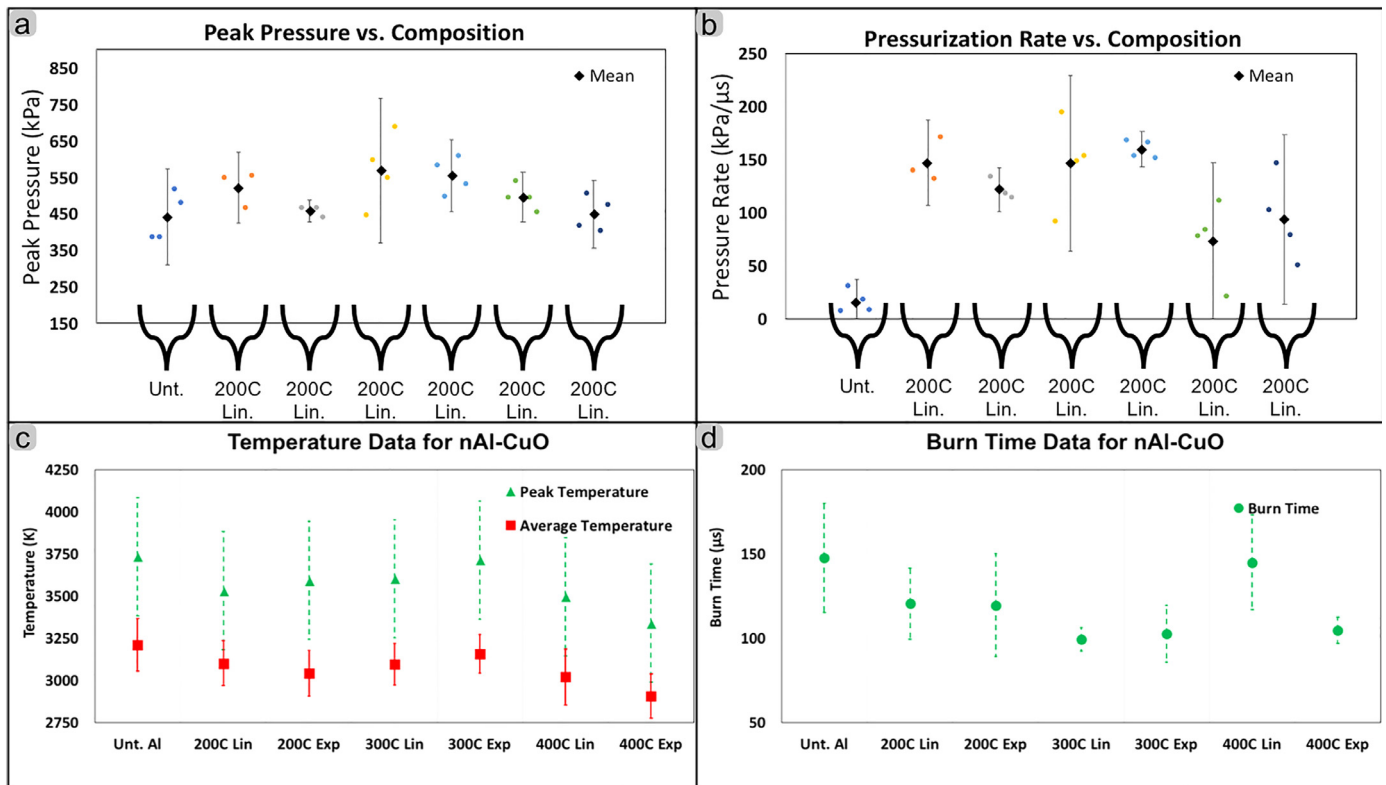


**Fig. 1.** Pressure cell data showing effect of prestressing (a) on peak pressure and (b) on pressurization rate. Error bars represent 95% confidence interval; (c) on temperature; and (d) on burn time. Note that prestressing conditions on the x-axis are indicated by the annealing temperature in  $^{\circ}\text{C}$  followed by the quenching rate shown as exponential (Exp) or Linear (Lin) corresponding to slower and faster quenching, respectively. Also note that vertical lines encompassing data points indicate one standard deviation in the measurements.

to fracture or become phase-inhomogeneous at annealing temperatures beyond  $300^{\circ}\text{C}$ . It is unlikely that the active aluminum content of the nAl particles deteriorated during prestressing, given that annealing was performed in nitrogen. But, previous TGA results on nAl reactions in air demonstrate the nAl reaction onset could be as low as  $450^{\circ}\text{C}$  [44]. In this case, particles with fractured shells subsequent to prestressing may heal when exposed to an ambient air environment such that the active aluminum content may diminished.

Temperature measurements (in K) made during the constant volume combustion of the composites are shown in Fig. 1c. The light emission from the reaction was fit to Planck's law with grey body assumption. The peak temperatures approach  $\sim 3800\text{K}$ , which can be expected from the combustion of aluminum in gaseous oxygen, given that CuO decomposes to  $\text{Cu}_2\text{O}$  and oxygen [36]. The peak temperatures were thresholded to the highest admissible error ( $\pm 350\text{K}$ ), which made meaningful mechanistic interpretation difficult. The average temperatures, on the other hand, have much lower error compared to peak temperatures, and with prestressing, the average temperatures are slightly lower than for the untreated samples. Further discussion about the ramifications of the temperature dependence can be found in a later section. For the  $400^{\circ}\text{C}$  annealing condition, the peak and average temperatures were lower than for the other samples, which in conjunction with the poor pressure metrics, reinforce the detrimental effects on the active content that may result from jeopardizing the integrity of the alumina shell. The full width half max (FWHM) burn time obtained from the integrated emission spectra during reaction is shown in Fig. 1d, where the samples annealed to  $200^{\circ}\text{C}$  and  $300^{\circ}\text{C}$  show faster burn times compared to the untreated and  $400^{\circ}\text{C}$  samples. Also evident is the inverse correlation between burn time and peak pressure measurements, which would imply that the

samples annealed to  $200^{\circ}\text{C}$  and  $300^{\circ}\text{C}$  achieve a more complete reaction given that they attain higher peak pressure and faster combustion despite having the same composition [6].

### 3.2. Hot stage, high heating rate in-situ microscopy

Select aluminum particles (without oxidizer) were tested in a high heating rate TEM where the samples were drop cast onto special microscopy grids and were subsequently ramped from room temperature (RT) to  $1200^{\circ}\text{C}$  at a rate of  $5 \times 10^5^{\circ}\text{C/s}$ . The heating rate and temperatures were selected to mimic actual experimental conditions, where reaction time scales are observed to be on the order of  $100\ \mu\text{s}$  (Fig. 1c). The results for untreated nAl are shown in Fig. 2a–c whereas for the nAl annealed at  $300^{\circ}\text{C}$ -Exp are shown in Fig. 2d–f. Samples prior to heating pulse, as shown in Fig. 2a,d for nAl and  $300^{\circ}\text{C}$ -Exp samples respectively, exhibit a fairly aggregated structure. Upon being subjected to the rapid heating ramp, the morphology of the  $300^{\circ}\text{C}$  annealed sample (Fig. 2e) is observed to undergo significant changes, with the aluminum in the core appearing to diffuse out of the shell, leading to a reduction in the boundaries that clearly demarcated the individual nanoparticles prior to heating. No violent spallation/ejection of the core material is observed. Figure 2f shows a magnified image of the nanoparticles after the heating pulse showing heterogeneities in the shell leading to a more corrugated structure [43]. In contrast untreated nAl is observed to undergo no significant morphological changes post the rapid heating pulse (Fig. 2b), with some nanoparticles in the image undergoing contrast change, probably due to crystallization or healing of the defects in the shell at the high temperature. In order to force a morphological change as seen for the annealed samples, the nAl samples were subjected to a second heating ramp with a 1 s hold at  $1200^{\circ}\text{C}$ , which resulted

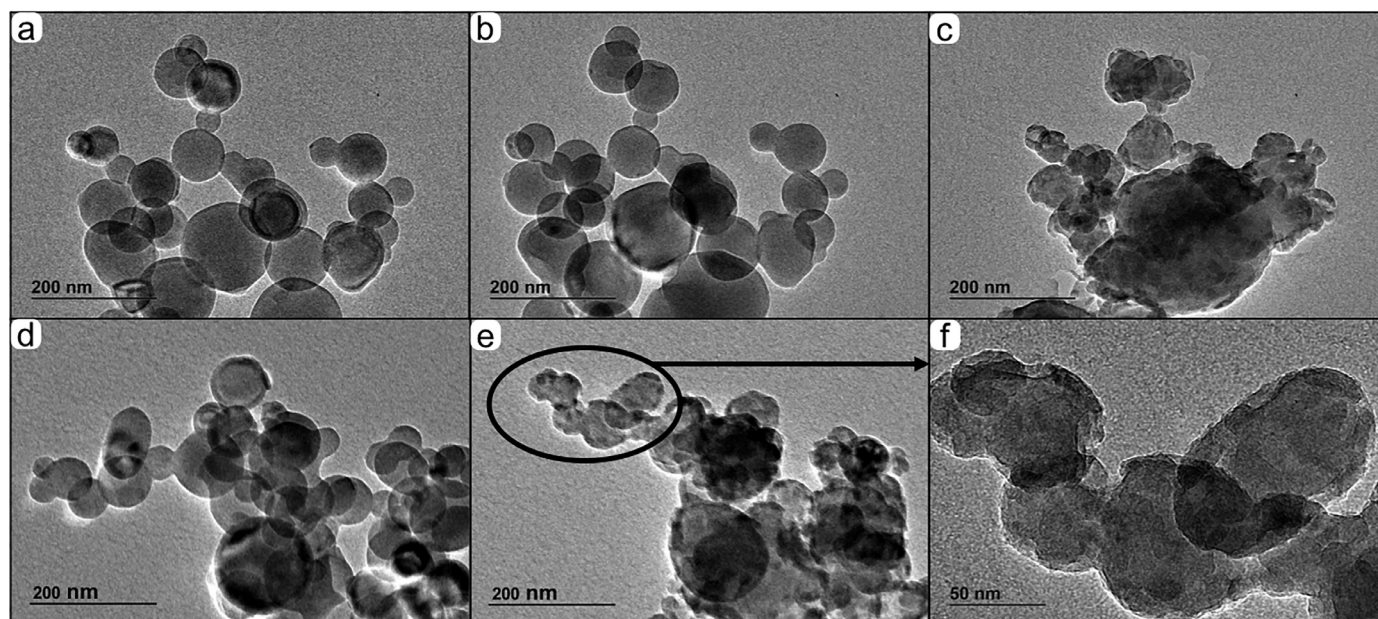


**Fig. 2.** High heating rate TEM results for untreated nAl (a) prior to heating, (b) after RT- 1200 °C ramp @ 5e5 K/s, (c) after RT- 1200 °C second ramp @ 5e5 K/s and hold for 1 s; and for 300 °C Exp nAl (d) prior to heating, (e) after RT- 1200 °C ramp @ 5e5 K/s, (f) magnified image of (e) showing the shell structure.

**Table 1**

Strain measurement on Al core for nAl particles annealed to 300 °C and quenched at exponential and linear rates.

Strain, $\epsilon$ ( $\times 10^{-4}$ )		
Untreated	300 °C Exp	300 °C Lin
$0.69 \pm 0.04$	$6.66 \pm 1.34$	$5.56 \pm 0.90$

in significant morphological changes to the aggregate structure. Results in Fig. 2 imply that in case of prestressing, there is a greater propensity for the aluminum core to diffuse out of the shell when compared to that of the untreated Al samples.

### 3.3. X-ray diffraction

In order to quantify the internal strain in the particles after annealing, the nAl powder with 300 °C anneal condition was evaluated by powder X-ray diffraction analysis. For the 111, 200, and 220 aluminum reflections, a *Pseudo-Voigt* profile was fit to an  $R^2$  value greater than 0.995 from which the center point was extracted to obtain the lattice parameter. Comparison to the unstrained, theoretical value at standard conditions gives the strain produced in the sample, as shown in Table 1. There is an order of magnitude difference in strain compared to the untreated sample for both cooling conditions.

## 4. Discussion

Results presented in Fig. 1 demonstrate the benefits of prestressing nAl particles prior to combustion, with the prestressed nAl+CuO composites achieving higher peak pressure, higher pressurization rates and faster burn times compared to the untreated nAl+CuO. Bachmaier and Pippan [27] demonstrated a significant reduction in hardness when consolidated pellets of micron aluminum particles (1.3  $\mu\text{m}$ ) were annealed above 200 °C and attributed the reduction in hardness to the onset of grain growth determined through microscopy measurements. Recent results on prestressed micron aluminum revealed significant increase (an order of magnitude) in the measured dilatational strain in the

aluminum core when annealed at 300 °C, which would imply that the expanded aluminum core is inducing an elevated stress state with the core-shell structure [26]. The shell is amorphous and XRD measurements of the strain and stress within the shell are not possible, but the core is crystalline, and Table 1 shows that for nAl particles annealed to 300 °C, the strain is an order of magnitude higher than the untreated nAl. Similar results corroborating the expanding nAl core were also observed in hot stage TEM experiments and concluded that the untreated aluminum core was initially expanded at room temperature under tension and passes through a zero-strain state at  $\sim 300$  °C, followed by an unconstrained expansion above 300 °C. This was facilitated by the inhomogeneities developed in the shell due to phase changes in alumina and/or penetration of Al ions that modifies its microstructure [30]. Molecular dynamics simulations [10] on nAl particles revealed the presence of induced electric fields at the core-shell interface (Cabrera Mott mechanism) that aid the transfer of aluminum ions across the shell, culminating in softening of the nanoparticle shell. The softened shell is postulated to melt at a lower temperature which combined with the softer aluminum core (due to grain growth during annealing) could lead to faster release of aluminum, as exemplified by the TEM results in Fig. 2, where a significant loss of nanostructure is observed under reduced thermal load for the annealed samples as opposed to the untreated nAl samples.

Owing to the observed loss in nanostructure, we believe the previously postulated condensed phase exothermic reactive sintering mechanism, aided by species diffusion, is dominant in these prestressed nAl composites [45]. The mechanism is predicated on the reactant moieties attaining significant mobility in the condensed phase such that they diffuse rapidly toward each other resulting in a reaction interface. The heat generated at the interface is transmitted through the sample, leading to further melting of the unreacted samples. The molten reactants are subsequently transferred toward the interface through capillary forces which propagate the reaction. High resolution TEM and macro scale product collection techniques have revealed the presence of such reaction interfaces within the composite [14,15]. Also, the strain manifested in prestressed samples are an order of magnitude larger than the untreated case (Table 1), which corresponds to a tensile stress in the aluminum core. The TEM images in Fig. 2 show

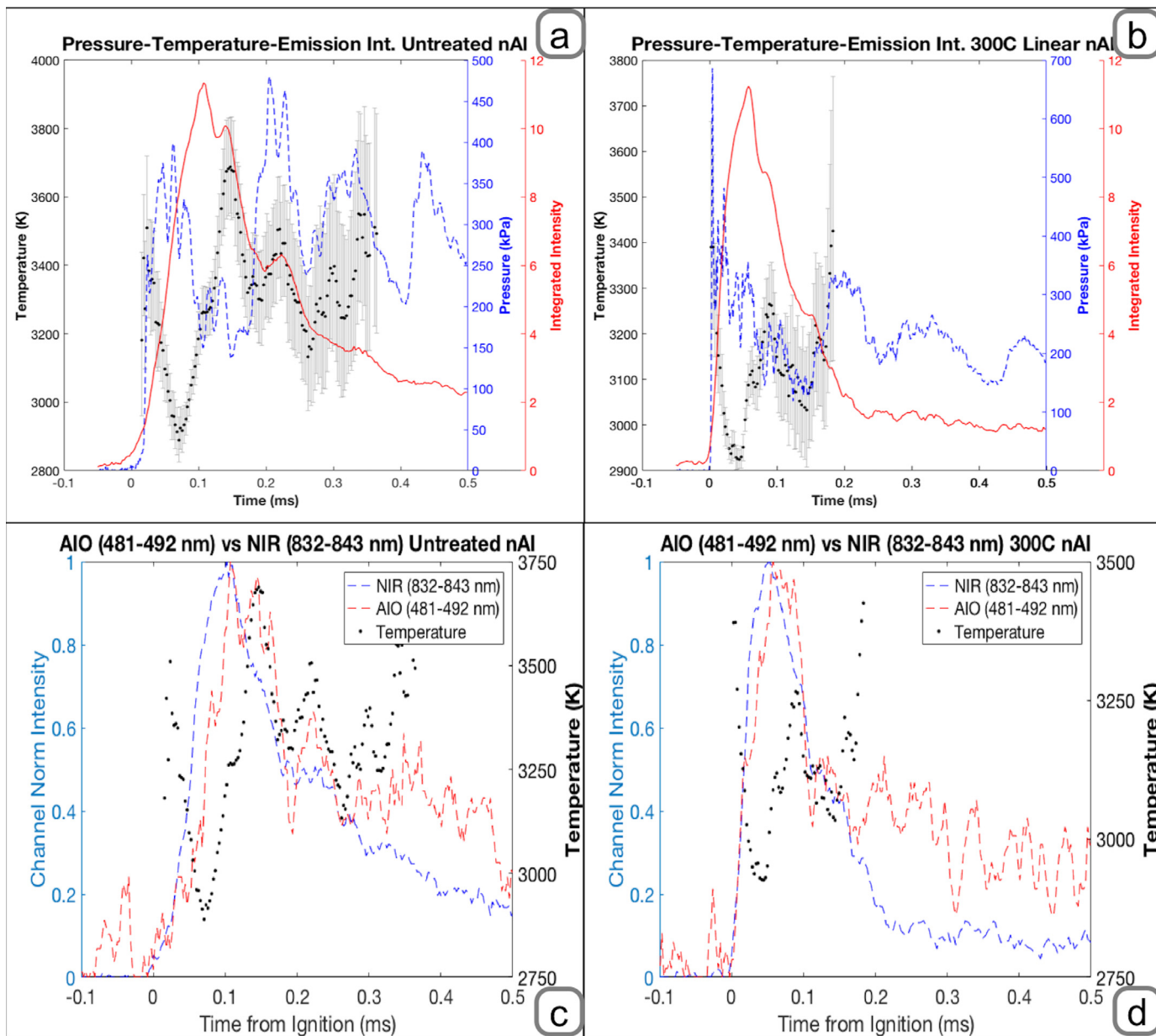


Fig. 3. Pressure-temperature and emission data for (a) untreated nAl and (b) 300°C linear nAl; NIR vs AIO channel profile for (c) untreated nAl and (d) 300°C linear nAl.

that aluminum release occurred faster in the prestressed samples, which is likely a consequence of the larger internal stresses generated from annealing and quenching compromising the shell, leading to its failure. This idea is further corroborated by the morphological changes experienced by the untreated sample during its second heating pulse. It is likely that the first pulse weakened the oxide shells (either through crack formation or inhomogeneous crystallization), and the second pulse allowed aluminum to leak out of the particles after an extended hold at elevated temperature.

A faster release of aluminum for the prestressed samples is reflected in temporal combustion behavior, as demonstrated in Fig. 3a,b, where the pressure, emission and temperature (with grey error bars) from the reaction in the combustion vessel is plotted temporally for untreated and 300 °C annealing condition with faster (linear) quenching. The time axis is truncated at 0.5 ms because the emission intensity is observed to drop significantly beyond 0.5 ms resulting in high errors in measured temperatures.

As can be clearly seen in Fig. 3a, for untreated samples, the pressure profile is oscillatory whereas for the 300 °C (Lin) sample, in Fig. 3b, the initial pressure is violent spike with a rapid decay implying a more rapid reaction. This qualitatively can also be seen from the emission profile which is clearly narrower for the prestressed material. In Fig. 3a, the temperature fits (with grey error bars) are also shown where, upon ignition, the sample temperature is observed to increase followed by a rapid drop to ~2900K just before peak emission. With the adiabatic flame temperature of Al + CuO calculated to be 2967 K [46], this region should correspond to the combustion of the bulk of the composite following which the temperature is observed to rise to ~3500 K. The temperature profile superimposed on the normalized emission intensity of two channels of the spectrometer is shown in Fig. 3c (Untreated nAl) and Fig. 3d (300 °C Lin), respectively. The channels were specifically chosen to compare the thermal component of emission with that of AIO ( $B^2\Sigma^+ \rightarrow X^2\Sigma^+ + \Delta v = 0$  band) [47]. For the thermal component, the channel covering a band from

832–843 nm (NIR) was chosen, devoid of any molecular emission. For the AlO channel, a band of 481–492 nm was chosen.

Qualitatively, the normalized spectral emission from the aforementioned channels show no significant deviation from each other during peak emission, which would suggest the predominance of thermal events during this time scale. At longer durations, as the emission intensity decreases, significant deviations between the emission profiles are observed for both the untreated (Fig. 3c) and 300 °C Linear (Fig. 3d) samples, which would suggest significant contributions from molecular emissions of AlO. This is expected given that CuO has the propensity to decompose into gaseous oxygen [36] which could react with aluminum in the gas phase. [48] Owing to the low resolution of the spectra, no direct fits to the molecular emission could be made to infer gas phase temperatures, but owing to the strength of the AlO emission, temporal comparisons can be used to make inferences on the reaction mechanism. Although the reaction temperatures are similar for the two samples shown in Fig. 3, it can be qualitatively observed that for the untreated nAl case, the emission profile is observed to be wider than for the 300 °C (Lin) sample. Moreover, for the untreated samples (Fig. 3a), the temperature is observed to attain maxima (~3700K) simultaneously with the net emission, whereas for the prestressed case, the peak temperature is observed after significant reduction in the total emission (Fig. 3b). Such high temperature peaks also correspond to local deviations between the NIR and AlO channels as shown in Fig. 3c–d, suggesting the presence of gas phase reactions, which is plausible given that shock tube measurements have shown that aluminum nanoparticles burn at ~3500K in high pressure, high oxygen environments [49]. Moreover, such high temperatures also resemble micron aluminum combustion temperatures in ambient environments, which may suggest that the nanoparticles are coalescing into larger (>80 nm) droplets and subsequently reacting with the oxygen [50]. The observation that the reaction temperature of prestressed samples are closer to the adiabatic flame temperature of the Al-CuO reaction for significant portion of the total emission suggests a higher contribution of the thermite reaction as opposed to aluminum reacting with gaseous oxygen from CuO decomposition. In both cases, the AlO channel is observed to decay slower than the NIR channel. Although the noise level in the AlO channel is high, it highlights the late gas phase combustion between aluminum and oxygen with the aluminum presumably larger (>80 nm) droplets.

Upon further increase in the annealing temperature to 400 °C, the pressure response of the sample deteriorates significantly (see Fig. 1a). A possible reason for this behavior could be imperfections induced within the alumina shell due to phase transitions or fracturing, which could affect the integrity of the shell. Diminishing the integrity of the shell could lead to multiple effects on reactivity, for example, without a pristine shell to constrain expansion of the core the stress level of the particle would not be elevated to levels observed for the 300 °C annealing conditions (see Table 1). The elevated stress state may catalyze the diffusion mechanism by promoting mass transfer or perhaps an electro potential difference (Cabrera Mott) that contribute to accelerated diffusion. Without an elevated stress, these mechanisms may not be activated. Also, cracks in the shell may heal once the powder is exposed to ambient air conditions and could influence reduced active aluminum content. The measured temperatures of the nAl 400 °C annealing conditions are also slightly lower than the other samples (Fig. 1b), which could possibly be the result of the composite being fuel lean owing to loss of active aluminum after prestressing. Although direct estimation of the governing factors in combustion of prestressed nAl could not be made, there is merit in prestressing nAl particles for improving reactivity and is a strategy worth exploring owing to its simplicity and ease of scale up, given that commercially manufactured material could be directly used.

## 5. Conclusions

We observe that prestressing nanoaluminum (nAl) powder is an approach to altering the mechanical properties of the core-shell particle structure that influences combustion. This study focused on examining the reactivity of prestressed nAl with copper oxide powder (nAl + CuO). Results show that prestressing results in increased peak pressure and pressurization rate compared with untreated nAl. Annealing at 300 °C with linear (faster) quenching resulted in the most optimal combustion performance. Annealing at 400 °C diminished material reactivity and it is theorized that inhomogeneities generated within the alumina passivation shell during annealing inhibit stress formation that accelerates the reaction mechanism. Flame temperatures measured were consistent between all samples but burn times were measurably reduced for prestressed nAl with 300 °C annealing conditions, suggesting an increase in reactivity without changing the reaction mechanism. High heating rate hot stage TEM analysis revealed significant microstructural changes and loss of nanostructure at lower thermal loads for prestressed nAl composites. The analysis revealed that reactive sintering may be aided by core aluminum attaining greater mobility in the condensed phase due to softening of the core resulting from higher tensile strain sustained by the core during prestressing. The measured strain is an order of magnitude greater for prestressed nAl particles annealed to 300 °C compared to untreated nAl. These results suggest that mechanical manipulation of fuel particles may offer interesting opportunities to tune energy release profiles.

## Acknowledgments

The authors from Texas Tech are grateful to the Office of Naval Research (ONR) and our Program Manager, Dr. Chad Stoltz, for support and encouragement under grant numbers N00014-16-1-2079. The authors from the University of Maryland are grateful for the support of the Army Research Office, and Dr. Ralph Anthenien.

## Supplementary materials

Supplementary material associated with this article can be found, in the online version, at doi:10.1016/j.combustflame.2019.03.024.

## References

- [1] C.M. Drew, A.S. Gordon, R.H. Knipe, Study of quenched aluminum particle combustion, in: H.G. Wolfhard, I. Glassman, L. Green Jr. (Eds.), *Heterogeneous Combustion*, 1964, pp. 17–39.
- [2] D. Sundaram, V. Yang, R.A. Yetter, Metal-based nanoenergetic materials: synthesis, properties, and applications, *Prog. Energy Combust. Sci* 61 (2017) 293–365.
- [3] M.W. Beckstead, Correlating aluminum burning times, *Combust. Explos. Shock Waves* 41 (2005) 533–546.
- [4] Y. Huang, G.A. Risha, V. Yang, R.A. Yetter, Effect of particle size on combustion of aluminum particle dust in air, *Combust. Flame* 156 (2009) 5–13.
- [5] K.T. Sullivan, J.D. Kuntz, A.E. Gash, The role of fuel particle size on flame propagation velocity in thermites with a nanoscale oxidizer, *Propellants Explos. Pyrotech.* 39 (2014) 407–415.
- [6] K.J. Hill, J. Warzywoda, M.L. Pantoya, V.I. Levitas, Dropping the hammer: examining impact ignition and combustion using pre-stressed aluminum powder, *J. Appl. Phys.* 122 (2017) 125102.
- [7] J.J. Granier, K.B. Plantier, M.L. Pantoya, The role of the Al<sub>2</sub>O<sub>3</sub> passivation shell surrounding nano-Al particles in the combustion synthesis of NiAl, *J. Mater. Sci.* 39 (2004) 6421–6431.
- [8] G.C. Egan, K.T. Sullivan, T. Lagrange, B.W. Reed, M.R. Zachariah, In situ imaging of ultra-fast loss of nanostructure in nanoparticle aggregates, *J. Appl. Phys* 115 (2014).
- [9] Y. Zong, R.J. Jacob, S. Li, M.R. Zachariah, Size resolved high temperature oxidation kinetics of nano-sized titanium and zirconium particles, *J. Phys. Chem. A*. 119 (2015) 6171–6178.
- [10] P. Chakraborty, M.R. Zachariah, Do nanoenergetic particles remain nano-sized during combustion? *Combust. Flame* 161 (2014) 1408–1416.

- [11] S. Chowdhury, K. Sullivan, N. Piekielek, L. Zhou, M.R. Zachariah, Diffusive vs explosive reaction at the nanoscale, *J. Phys. Chem. C* 114 (2010) 9191–9195.
- [12] V.I. Levitas, M.L. Pantoya, S. Dean, Melt dispersion mechanism for fast reaction of aluminum nano- and micron-scale particles: flame propagation and SEM studies, *Combust. Flame* 161 (2014) 1668–1677.
- [13] M.A. Trunov, M. Schoenitz, E.L. Dreizin, Effect of polymorphic phase transformations in alumina layer on ignition of aluminium particles, *Combust. Theory Model.* 10 (2006) 603–623.
- [14] G.C. Egan, T. Lagrange, M.R. Zachariah, Time-resolved nanosecond imaging of nanoscale condensed phase reaction, *J. Phys. Chem. C* 119 (2015) 2792–2797.
- [15] R.J. Jacob, D.L. Ortiz-Montalvo, K.R. Overdeep, T.P. Weihs, M.R. Zachariah, Incomplete reactions in nanothermite composites, *J. Appl. Phys.* 121 (2017).
- [16] R.J. Jacob, G. Jian, P.M. Guerieri, M.R. Zachariah, Energy release pathways in nanothermites follow through the condensed state, *Combust. Flame* 162 (2015) 258–264.
- [17] X. Zhou, M. Torabi, J. Lu, R.Q. Shen, K.L. Zhang, Nanostructured energetic composites: synthesis, ignition/combustion modeling, and applications, *ACS Appl. Mater. Interfaces* 6 (2014) 3058–3074.
- [18] H. Wang, R.J. Jacob, J.B. DeLisio, M.R. Zachariah, Assembly and encapsulation of aluminum NP's within AP/NC matrix and their reactive properties, *Combust. Flame* 180 (2017) 175–183.
- [19] K.-L. Chintersingh, M. Schoenitz, E.L. Dreizin, Combustion of boron and boron-iron composite particles in different oxidizers, *Combust. Flame* 192 (2018) 44–58.
- [20] A. Epshteyn, M.R. Weismiller, Z.J. Huba, E.L. Maling, A.S. Chaimowitz, Optimization of a high-energy Ti-Al-B nanopowder fuel, *Energy Fuels* 31 (2017) 1811–1819.
- [21] Y. Yao, Z. Huang, P. Xie, S.D. Lacey, R.J. Jacob, H. Xie, F. Chen, A. Nie, T. Pu, M. Rehwoldt, D. Yu, M.R. Zachariah, C. Wang, R. Shahbazian-Yassar, J. Li, L. Hu, Carbothermal shock synthesis of high-entropy-alloy nanoparticles, *Science* 359 (2018) 1489–1494.
- [22] W.K. Lewis, C.G. Rumchik, M.J. Smith, K.A.S. Fernando, C.A. Crouse, J.E. Spowart, E.A. Gulians, C.E. Bunker, Comparison of post-detonation combustion in explosives incorporating aluminum nanoparticles: influence of the passivation layer, *J. Appl. Phys.* 113 (2013).
- [23] K.S. Kappagantula, M.L. Pantoya, J. Horn, Effect of surface coatings on aluminum fuel particles toward nanocomposite combustion, *Surf. Coatings Technol.* 237 (2013) 456–459.
- [24] R.J. Helmich, K.S. Suslick, Chemical aerosol flow synthesis of hollow metallic aluminum particles, *Chem. Mater.* 22 (2010) 4835–4837.
- [25] D. Prentice, M.L. Pantoya, A.E. Gash, Combustion wave speeds of sol-gel-synthesized tungsten trioxide and nano-aluminum: the effect of impurities on flame propagation, *Energy Fuels* 20 (2006) 2370–2376.
- [26] J. McCollum, D.K. Smith, K.J. Hill, M.L. Pantoya, J. Warzywoda, N. Tamura, A slice of an aluminum particle: examining grains, strain and reactivity, *Combust. Flame* 173 (2016) 229–234.
- [27] A. Bachmaier, R. Phippan, Effect of oxide particles on the stabilization and final microstructure in aluminium, *Mater. Sci. Eng. A* 528 (2011) 7589–7595.
- [28] V.I. Levitas, B. Dikici, M.L. Pantoya, Toward design of the pre-stressed nano- and microscale aluminum particles covered by oxide shell, *Combust. Flame* 158 (2011) 1413–1417.
- [29] B. Dikici, M.L. Pantoya, V. Levitas, The effect of pre-heating on flame propagation in nanocomposite thermites, *Combust. Flame* 157 (2010) 1581–1585.
- [30] D.A. Firmansyah, K. Sullivan, K.S. Lee, Y.H. Kim, R. Zahaf, M.R. Zachariah, D. Lee, Microstructural behavior of the alumina shell and aluminum core before and after melting of aluminum nanoparticles, *J. Phys. Chem. C* 116 (2012) 404–411.
- [31] S. Timoshenko, Analysis of Bi-metal thermostats, *J. Opt. Soc. Am.* 11 (1925) 233.
- [32] J.F. Throop, J.H. Underwood, G.S. Leger, Thermal relaxation in autofretted cylinders, in: E. Kula, V. Weiss (Eds.), *Residual Stress Stress Relax*, Springer, US, Boston, MA, 1982, pp. 205–226.
- [33] M.R. James, Relaxation of residual stresses – an overview, *Residual Stresses*, 1987, pp. 349–365.
- [34] D. Pesiri, C. Aumann, L. Bilger, D. Booth, R.D. Carpenter, R. Dye, E. O'Neill, D. Shelton, K.C. Walter, Industrial scale nano-aluminum powder manufacturing, *J. Pyrotech* 19 (2004) 19–31.
- [35] Personnel communication with Dr. Kurt Schroder, Novacentrix, Austin, TX., (2014).
- [36] G.Q. Jian, S. Chowdhury, K. Sullivan, M.R. Zachariah, Nanothermite reactions: is gas phase oxygen generation from the oxygen carrier an essential prerequisite to ignition? *Combust. Flame* 160 (2013) 432–437.
- [37] C.D. Yarrington, S.F. Son, T.J. Foley, S.J. Obrey, A.N. Pacheco, Nano aluminum energetics: the effect of synthesis method on morphology and combustion performance, *Propellants Explos. Pyrotech.* 36 (2011) 551–557.
- [38] J. McCollum, M.L. Pantoya, N. Tamura, Improving aluminum particle reactivity by annealing and quenching treatments: synchrotron X-ray diffraction analysis of strain, *Acta Mater.* 103 (2016) 495–501.
- [39] R.J. Jacob, D.J. Kline, M.R. Zachariah, High speed 2-dimensional temperature measurements of nanothermite composites: probing thermal vs. gas generation effects, *J. Appl. Phys.* 123 (2018) 115902.
- [40] J. Kalman, D. Allen, N. Glumac, H. Krier, Optical depth effects on aluminum oxide spectral emissivity, *J. Thermophys. Heat Transf.* 29 (2015) 74–82.
- [41] P. Lynch, H. Krier, N. Glumac, Emissivity of aluminum-oxide particle clouds: application to pyrometry of explosive fireballs, *J. Thermophys. Heat Transf.* 24 (2010) 301–308.
- [42] MATLAB and Statistics Toolbox Release (v2012), (2012).
- [43] K.T. Sullivan, W.A. Chiou, R. Fiore, M.R. Zachariah, In situ microscopy of rapidly heated nano-Al and nano-Al/WO<sub>3</sub> thermites, *Appl. Phys. Lett.* 97 (2010) 133104.
- [44] B. Rufino, F. Boulc'h, M.V. Coulet, G. Lacroix, R. Denoyel, Influence of particles size on thermal properties of aluminium powder, *Acta Mater.* 55 (2007) 2815–2827.
- [45] K.T. Sullivan, N.W. Piekielek, C. Wu, S. Chowdhury, S.T. Kelly, T.C. Hufnagel, K. Fezzaa, M.R. Zachariah, Reactive sintering: an important component in the combustion of nanocomposite thermites, *Combust. Flame* 159 (2012) 2–15.
- [46] K. Sullivan, M.R. Zachariah, Simultaneous pressure and optical measurements of nanoaluminum thermites: investigating the reaction mechanism, *J. Propuls. Power* 26 (2010) 467–472.
- [47] C.G. Parigger, J.O. Hornkohl, Computation of AlO B<sub>2</sub>Σ<sup>+</sup> X<sub>2</sub>Σ<sup>+</sup> emission spectra, *Spectrochim. Acta - Part A Mol. Biomol. Spectrosc.* 81 (2011) 404–411.
- [48] P. Lynch, G. Fiore, H. Krier, N. Glumac, Gas-phase reaction in nanoaluminum combustion, *Combust. Sci. Technol.* 182 (2010) 842–857.
- [49] T. Bazyn, H. Krier, N. Glumac, Combustion of nanoaluminum at elevated pressure and temperature behind reflected shock waves, *Combust. Flame* 145 (2006) 703–713.
- [50] P. Bucher, R.A. Yetter, F.L. Dryer, T.P. Parr, D.M. Hanson-Parr, PLIF species and ratiometric temperature measurements of aluminum particle combustion in O<sub>2</sub>, CO<sub>2</sub> and N<sub>2</sub>O oxidizers, and comparison with model calculations, *Symp. (Int.) Combust.* 27 (1998) 2421–2429 Vols 1 2.